Cellular/Molecular

Identification of the Acid-Sensitive Site Critical for Chloral Hydrate (CH) Activation of the Proton-Activated Chloride Channel

Xiang-Ying Xu,[1,2,3]* Fei-Fei Zhang,[1,2,3]* Jun Gan,[1,2,3] Mao-Yin Zhang,[4] Zhong-Shan Shen,[1,2,3] Qing Guo,[1,2,3] Yue Teng,[1,2,3] Jun-Wei Ji,[1,2,3] Jun-Li Cao,[1,2,3] Qiong-Yao Tang,[1,2,3] and Zhe Zhang[1,2,3]

[1]Jiangsu Province Key Laboratory of Anesthesiology, Xuzhou Medical University, Xuzhou, Jiangsu Province 221004, China, [2]Jiangsu Province Key Laboratory of Anesthesia and Analgesia Application Technology, Xuzhou Medical University, Xuzhou, Jiangsu Province 221004, China, [3]NMPA Key Laboratory for Research and Evaluation of Narcotic and Psychotropic Drugs, Xuzhou Medical University, Xuzhou, Jiangsu Province 221004, China, and [4]Department of Anesthesiology, the Affiliated Hospital of Xuzhou Medical University

The transmembrane protein TMEM206 was recently identified as the molecular basis of the extracellular proton-activated Cl^- channel (PAC), which plays an essential role in neuronal death in ischemia-reperfusion. The PAC channel is activated by extracellular acid, but the proton-sensitive mechanism remains unclear, although different acid-sensitive pockets have been suggested based on the cryo-EM structure of the human PAC (hPAC) channel. In the present study, we firstly identified two acidic amino acid residues that removed the pH-dependent activation of the hPAC channel by neutralization all the conservative negative charged residues located in the extracellular domain of the hPAC channel and some positively charged residues at the hotspot combined with two-electrode voltage-clamp (TEVC) recording in the *Xenopus* oocytes system. Double-mutant cycle analysis and double cysteine mutant of these two residues proved that these two residues cooperatively form a proton-sensitive site. In addition, we found that chloral hydrate activates the hPAC channel depending on the normal pH sensitivity of the hPAC channel. Furthermore, the PAC channel knock-out (KO) male mice (C57BL/6J) resist chloral hydrate-induced sedation and hypnosis. Our study provides a molecular basis for understanding the proton-dependent activation mechanism of the hPAC channel and a novel drug target of chloral hydrate.

Key words: biophysical mechanism; chloral hydrate; PAC; pH sensitivity; TEVC

Significance Statement

Proton-activated Cl^- channel (PAC) channels are widely distributed in the nervous system and play a vital pathophysiological role in ischemia and endosomal acidification. The main discovery of this paper is that we identified the proton activation mechanism of the human proton-activated chloride channel (hPAC). Intriguingly, we also found that anesthetic chloral hydrate can activate the hPAC channel in a pH-dependent manner. We found that the chloral hydrate activates the hPAC channel and needs the integrity of the pH-sensitive site. In addition, the PAC channel knock-out (KO) mice are resistant to chloral hydrate-induced anesthesia. The study on PAC channels' pH activation mechanism enables us to better understand PAC's biophysical mechanism and provides a novel target of chloral hydrate.

Introduction

The TMEM206 has been recently identified as the gene that encodes the proton-activated Cl^- channel (PAC), which plays a vital role in neuronal death in ischemia-reperfusion (Yang et al., 2019). Although the molecular basis of the PAC channel was identified until recently, the study history on this channel could be traced back to the characterization of the proton-activated current in HEK293 cells (Lambert and Oberwinkler, 2005). The hPAC channel is endogenously expressed in HEK293 cells, which shows a proton-activated, outwardly rectifying anionic current (PAORAC) distinguished from volume-regulated anionic current (VRAC). The PAORAC channel single conductance is around

10–20 pS when depolarization voltage is between 50 and 130 mV (Lambert and Oberwinkler, 2005). The PAC channel is expressed in neurons, astrocytes, and microglia cells in the nervous system. Furthermore, the PAC channel is also expressed in other carcinoma cell lines, in which the PAC channel may promote the malignancy of cancers (Lambert and Oberwinkler, 2005; Kittl et al., 2019; Zhao et al., 2019; Zhang et al., 2020). Considering the PAC channels' wide expression, the PAC channel's function remains to be further explored.

Although the cryo-EM structures of PAC channels are available (Ruan et al., 2020; Deng et al., 2021), the biophysical property of the PAC channel remains to be further addressed. The PAC channel is composed of three pore-containing subunits. Each subunit possesses two transmembrane domains, with both N-terminus and C-terminus located intracellularly. Electrophysiological and biochemical studies identify the pore-containing subunit's topology (Ullrich et al., 2019). The ion-conducting pore of the PAC channel is lined by the β14, TM2 linker, and hydrophobic residues on TM2 (transmembrane domain). One extracellular gate at the extracellular domain (ECD) and transmembrane domain (TMD) junction and one transmembrane gate was suggested by cryo-EM and electrophysiological studies (Ullrich et al., 2019; Ruan et al., 2020; Deng et al., 2021). However, the pH-sensitive mechanisms of PAC channels are still bewildering because all mutations of the suggested pH-sensitive site by the earlier cryo-EM study fail to disrupt the PAC channel's sensitivity to extracellular proton. Based on a significant movement of H98 residue from the high-pH state to the low-pH proton bound state, the residue was predicted as a pH-sensitive site of the hPAC channel. However, the H98A, H98R, and another tested pH sensing residue's mutation, Q296A, are more sensitive to extracellular pH change than the wild-type (WT) type channel (Ruan et al., 2020), which argues against the idea that these residues are pH-sensitive sites. Another residue mutation, E107R, which is closed to H98 residue in the conformation obtained at pH 4.6, also shows stronger pH sensitivity. Another study that brought cryo-EM structure using the pufferfish PAC channel predicted an extracellular region containing several conserve titratable amino acids at the intersubunit interface as a pH sensor hotspot (Deng et al., 2021). But the mutations of these residues have not been tested.

In the present study, we performed a mutagenesis screening of the conservative negatively charged extracellular residues of the hPAC channel and alkalized residues in the hotspot to identify the possible pH-sensitive sites because the PAC channel sensitivity toward extracellular proton is conservative in all tested species (Ullrich et al., 2019). The electrophysiological data show two negatively charged residues completely disrupted the pH sensitivity of the hPAC channel. Further double mutant cycle analysis and double cysteine mutant show these two residues cooperate to form a pH-sensitive site. Interestingly, sedation medicine chloral hydrate activates the hPAC channel. This activation effect probably is realized by stabilizing the proton binding open conformation by chloral hydrate. Furthermore, the PAC channel knock-out (KO) mice are resistant to chloral hydrate-induced hypnosis, indicating the PAC channel is an essential target of the chloral hydrate.

Materials and Methods

Cloning the hPAC channel and RNA injection
We cloned the hPAC channel from a human brain cDNA library (A gift from Professor Xiuping Zhou, Xuzhou Medical University). We synthesized the first-Strand cDNA using the SuperScript First-Strand Synthesis Kit for RT-PCR (Invitrogen, 11904018) with an oligo d(T) primer. The hPAC gene was amplified by PCR using the cDNA library of the human

brain as a template. The primers for cloning the *hPAC* gene were: hPAC F1: 5′-AATTAAGGATCCATGATCCGGCAGGAGCGCT-3′ (The BamHI cleavage site is underlined); hPAC R1: 5′-AATTAACTCGAGTCA GCTTATGTGGCTCGTTGC (the XhoI cleavage site is underlined). After digesting with BamHI and XhoI, the PCR product was inserted into the pGEMSH vector between BamHI and XhoI sites under the control of the T7 promoter for transcription. The sequence was subsequently confirmed by DNA sequencing (gene ID: 55248). *hPAC* mutations were generated by Pfu-based mutagenesis using the Quick Change TM kit as the previously described procedure (G.M. Wang et al., 2020). NheI linearized the plasmids for in vitro transcription. RNA was transcribed using T7 polymerase (NEB), and cRNAs were prepared at a $\sim$ 0.5 × g/ml concentration. Each *Xenopus* oocyte was injected with 18.6–37.4 nl of hPAC mRNA. After 24 − 48 h, these oocytes were transferred to a recording chamber with a continuously perfused bath solution containing (in mM) 145 NaCl, 2 KCl, 2 MgCl₂, 1.5 CaCl₂, 10 HEPES, 10 glucose (300 mOsm/kg; pH 7.3 with NaOH). Different acidic pH solutions were composed of the same ionic components except replacing the HEPES with 5 mM Na₃-citrate. The pH values were titrated using citric acid.

Generating the hPAC-EGFP construct and hPAC flag-tagged constructs
For generating the hPAC-EGFP construct, the primers used for amplifying the *hPAC* gene were: hPAC F2: 5′-AATTAACTCGAGATGATCCG GCAGGCAGGAGCGCTCC-3′ (The NheI cleavage site is underlined); hPAC R2: 5′-AATTAAGGATCCCCGCTTATGTGGCTCGTTGCCTG-3′ (the BamHI cleavage site is underlined). The hPAC cDNA was amplified by PCR and recovered from an agarose gel after electrophoresis. The recovered DNA was cleaved by NheI and BamHI, and subsequently was cloned into a pEGFP-N1 vector for translation as a fused protein with EGFP. The *hPAC*-EGFP mutations were generated as previously described.

To obtain a construct with a Flag-tag at the C-terminal of the hPAC gene, the hPAC-FLAG fragment was amplified by PCR using the previously constructed plasmid pGEMSH-hPAC as a template. The primers for cloning the hPAC-FLAG fragment were PAC F: 5′-AATTAA GGATCCATGATCCGGCAGGAGCGCT-3′ (the BamH I cleavage site is underlined); PAC R: 5′-AATTAACTCGAGTCA*CTTATCGTCATCG TCTTTGTAAT*CGCTTATGTGGCTCGTTGCCTG-3′ (the XhoI cleavage site is underlined and FLAG tag sequences are in italic). The PCR product was digested with BamHI and XhoI and cloned into the same sites of the pCDNA3.1 and pGEMSH vectors, respectively.

Cell culture and transfection of hPAC-EGFP and hPAC-Flag tagged plasmids
In this study, HEK 293T cells were cultured in DMEM and 10% FBS (fetal bovine serum). The HEK293T cells were seeded at 2 × 10⁵/ml. The cells were cultured in laser confocal culture plates in an incubator at 37°C with 5% CO₂ until the cells reached 60–80% confluence. Then, the ExFect/DNA transfection mixture was prepared by adding 4 μg of each plasmid vector to 250-μl serum-free medium (Opti-MEM, Invitrogen, Thermo Fisher Scientific) and adding 10 μl of ExFect transfection reagent (Nanjing Vazyme Biotech Co) to 240-μl Opti-MEM. Twenty minutes after mixing, a volume of 500 μl of each transfection mixture was added to cell culture plates, and then the plates were shaken gently. Six hours after transfection, replaced the transfection mixture with DMEM with 10% FBS and incubated the cells at 37°C with 5% CO₂ for 48 h.

Wheat germ agglutinin (WGA) labeling and calculation of overlapping of the EGFP and WGA staining
Forty-eight hours after cell transfection, the cells were incubated with 5.0 μg/ml WGA Alexa Fluor 594 conjugate at 37°C for 10 min (Wheat Germ Agglutinin Conjugates, Invitrogen, Thermo Fisher Scientific). After incubation, the cells were washed twice with PBS to remove unbound WGA. Then, the cells were immersed in PBS and were observed under a confocal microscope Zeiss LSM880 for cell imaging. The percent colocalization of EGFP (green) and WGA

staining imaging (red) was calculated and demonstrated as overlapping rates using the ImageJ software. In brief, the images of the red and green channels are merged, and the color thresholds were set beside the RGB color shown in yellow. Then the overlap rate was calculated as yellow areas divided by green areas.

Electrophysiology

Oocytes preparation

Oocytes were used 1–3 d after RNA injection for two-electrode voltage-clamp (TEVC) or 3–6 d after RNA injection for outside-out patches. Stage IV *Xenopus laevis* oocytes were prepared according to protocols used in this laboratory, as previously described (Tang et al., 2016). The surgery protocol complied with Xuzhou Medical University's Institutional Animal Care and Use Committee (IACUC) guidelines. Before surgery, adult female *Xenopus laevis* frogs were anesthetized by tricaine at a concentration of 10 g/m³ in a tank for several minutes. Subsequently, frogs were taken out of the tank and placed on ice. Under aseptic conditions, a small incision was cut on one side of the abdomen to remove several pieces of ovarian lobes. The lobes were washed and placed in a sterile OR2 solution (in mM; 85 NaCl, 5 KCl, 5 HEPES-NaOH, and 1 MgCl₂, pH 7.0) supplemented with tetracycline (0.05 g/l; Sigma). Oocytes were defolliculated and shook in OR2 solution containing 2 mg/ml collagenase (Type II; Boehringer) at room temperature for 45 min and washed in ND96 solution (in mM, 96 NaCl, 2 KCl, 1 MgCl₂, and 5 HEPES, pH 7.5) at room temperature for another 1 h on a rotator (30 rpm).

Outside-out patch recording

The hPAC currents were recorded using an outside-out patch configuration using the PC2C amplifier (Yibo). Data were transferred and stored in a computer by the PUDA acquisition system (Yibo). Gigaohm seals were formed in ND96 solution (in mM; 96 NaCl, 2 KCl, 1.8 CaCl₂, 1 MgCl₂, 8 HEPES, and 2.5 sodium pyruvate, pH 7.5). Pipette solution containing (in mM): 135 CsCl, 1 MgCl₂, 2 CaCl₂, 10 HEPES, 5 EGTA, and 4 MgATP (280–290 mOsm/kg; pH 7.2 with CsOH). The perfusion solution at pH 7.3 containing (in mM): 145 NaCl, 2 KCl, 2 MgCl₂, 1.5 CaCl₂, 10 HEPES, and 10 glucose, titrated to pH 7.3 with NaOH. The perfusion solution at pH 5.5 and pH 4.6 containing (in mM): 145 NaCl, 2 KCl, 2 MgCl₂, 1.5 CaCl₂, 5 Na₃Citrate, and 10 glucose, titrated to pH 5.5 and pH 4.6 with citrate. Patch-clamp recording pipettes were made from borosilicate capillary tubes. Typical pipette resistance is 1–3 MΩ.

TEVC recording

The glass electrodes were prepared and filled with 3 M KCl agarose (1 g agarose in 100 ml 3 M KCl), then the pipettes were stored in a wet box at 4°C. The resistance of the voltage electrode is about 2 MΩ (<4 MΩ), and the resistance of the current electrode is ~1 MΩ. Currents were recorded by Oocyte clamp QC-725C amplifier (Warner Instruments) and by WinWCP software (Strathclyde Electrophysiology Software V5.5.5). Currents were obtained using a step potential protocol which steps from −100 to +200 mV with a 20-mV increment in each step. The oocyte incubation solution is as same as the perfusion solutions used in outside-out patch recordings. The chloral hydrate perfusion solution at pH 5.5 containing (in mM): 145 NaCl, 2 KCl, 2 MgCl₂, 1.5 CaCl₂, 5 Na₃Citrate, 10 glucose, and 100 chloral hydrate (approximate Osm 377), titrated to pH 5.5 with citrate, and then diluting into 10 mM (Osm 316), 20 mM (Osm 319), 25 mM (Osm 323), 50 mM (Osm 346), 75 mM (Osm 353). The osmolarity of the solution with 0 mM chloral hydrate is 307 Osm. The oocyte was put in the perfusion chamber (RC-3Z, Warner Instruments, Harvard
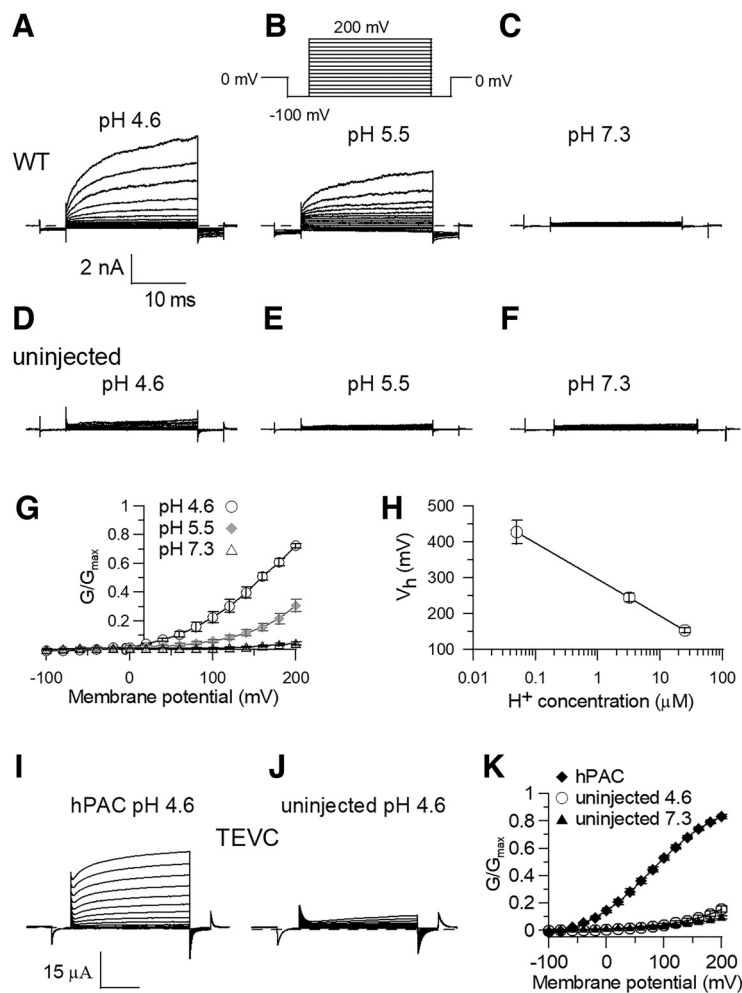

Figure 1. The pH and voltage-sensitive hPAC channel is expressed well in *Xenopus* oocytes. ***A–C***, Typical macroscopic current traces of the hPAC channel were recorded with outside-out voltage-clamp configuration in *Xenopus* oocytes. The patches were bathed with the same solution components at different pH. Current traces were recorded with a 20- mV step from −100 to +200 mV. ***D–F***, Typical current traces were recorded from uninjected oocytes with the same outside-out voltage-clamp configuration. ***G***, G/G_{max} of the hPAC channel at different voltages in the perfusion solutions with different pH values. Data are expressed as mean ± SEM of six patches. ***H***, The V_h changes of the hPAC channel with the pH increase of the perfusion solution. ***I, J***, The sample current of the hPAC channels and uninjected oocytes was recorded by TEVC at pH 4.6. ***K***, The plotted GVs generated from currents recorded from the hPAC channel injected and uninjected oocytes, respectively.

Bioscience Inc.) soaked in the perfusion solution. The perfusion solution volume in the chamber is around 700 μl. We use the multiple syringes perfusion system to stock the perfusion solution with different pH values. The perfusion system was connected to the oocyte chamber through soft plastic tubes and a manifold with a single output channel. The oocyte chamber was connected to a glass bottle through a soft output channel. A vacuum pump extracts the perfusion solution from the chamber to the bottle once the perfusion solution reaches the fixed height of the output channel. The solutions exchanged with different pH were controlled by gravity and clipping of the soft tubes. The shift from a given pH value to another pH solution is <10 s. The recording process was finished within 3 min for a given pH value. Current at –100 mV was substracted as leak current.

The 50 mM dithiothreitol (DTT) in pH 4.6 perfusion solution was freshly prepared. The 50 mM DTT was used to reduce disulfide bonds formed in the mutation E257C/D289C.

Animals

C57BL/6J and PAC KO (GemPharmatech Co. Ltd.) mice (male) on a C57BL/6J background were used in this experiment. Xuzhou Medical University Animal Care and Use Committee approved all animal care
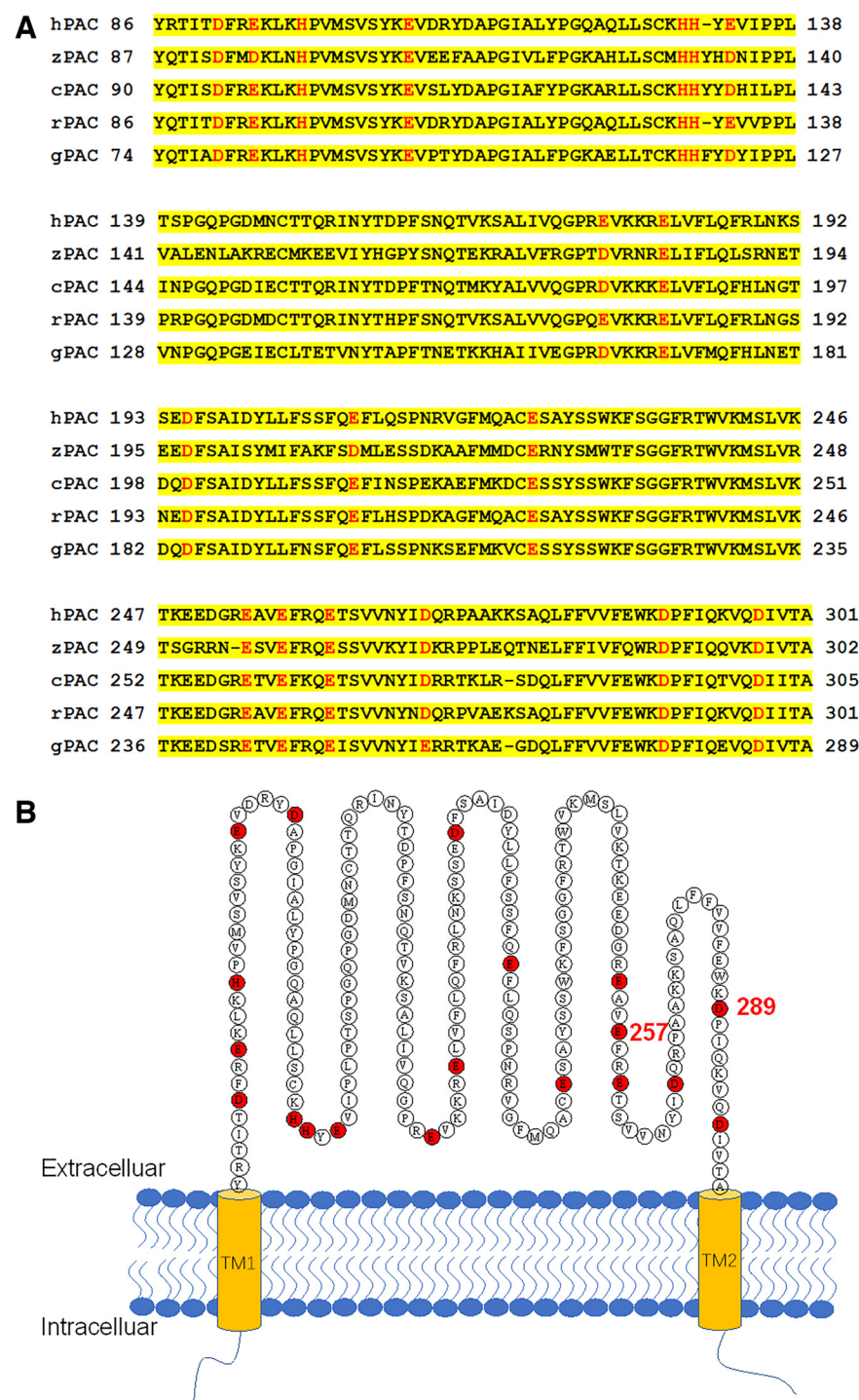
Figure 2. Alignment of the extracellular domain of the PAC channels. **A**, Alignment of amino acid sequences of the PAC orthologs that encode extracellular domain between TM1 and TM2. Residues shown in red color are conservative negative charged residues. The hPAC represents human TMEM206 (RefSeq: NM_018252.2; UniProtKB: Q9H813), zPAC (zebrafish TMEM206, RefSeq: NM_001291762.1; UniProtKB: X1WG42), cPAC (chicken TMEM206, RefSeq: XM_419431.6; UniProtKB: A0A1D5PSZ0), rPAC (naked mole rat TMEM206, RefSeq: XM_004853543.3; UniProtKB: A0A0N8ETT8), gPAC (green anole TMEM206, RefSeq: XM_003216011.3; UniProtKB: G1KFB8). **B**, The extracellular domain and the location of the conservative negative charged residues of the hPAC channel.

and experimental protocols. All procedures were performed following the *Guide for the Care and Use of Laboratory Animals* published by the National Institutes of Health (NIH Publication, eighth edition). The PAC channel KO mice were generated using the gRNA/Cas9 strategy (Fig. 9A) by GemPharmatech Co. Ltd. The genotyping was performed by PCR using the mouse tail genomic DNA as a template, genome

typing primers KO: 5′ primer: JS05329-Tmem206-5wttF2: CTTCCTCTAGGAAGTGG TTAGGACC; 3′ primer: JS05329-Tmem206-3wttR2: TGAGCAGTGAGGGAGACCTGTA TT. Target fragment 332 bp. Genotyping the WT mice: JS15329-Tmem206-wt-F2: CTTTG TGCATGTGTGACGGTTATGTG; JS15329-Tmem206-wt-R2: TTGAGACCCAACTCCA GGGTACAAGT. The WT mice fragment: 325 bp. Male mice aged 8–12 weeks were used in this study.

Membrane protein extraction and Western blotting
The membrane protein was extracted from HEK293T cells transfected by WT hPAC channel, E257Q, and D289N mutants with a kit (KeyGEN). The process was performed according to the manufacturer's protocol. First, we washed the plates of HEK293T cells twice with ice-cold PBS. Next, the dishes were added 1-ml lysis buffer containing 1‰ protease inhibitor cocktail and 1 mM DTT. We used a scraper to collect the cell lysates and pipetted them into a 1.5-ml Eppendorf tube. Then we gently vortexed cell lysates and incubated them on ice for 1 min. This process was repeated five times. Cytosolic proteins were separated by centrifugation at 12,000 rpm for 10 min at 4°C. Then we resuspended the pellets in the cold Extraction buffer, vortexed for 30 s, and placed them on ice for 5 min. Then, the process was repeated five times. Finally, membrane proteins were collected from the supernatant after centrifugation of the resuspended pellet at 12000 rpm for 10 min at 4°C. Protein concentration and yield were determined using the BCA Protein Assay kit (Beyotime). The membrane protein was extracted from *Xenopus* oocytes; ~30 *Xenopus* oocytes were homogenized with a homogenizer at 4°C in 1-ml lysis buffer containing 1‰ protease inhibitor cocktail and 1 mM DTT and then were incubated for 5 min on ice. The following procedure is the same as that used to extract membrane proteins from HEK293T cells.

One hundred micrograms of membrane protein were electrophoresed and transferred by SDS-PAGE using 12.5% (w/v) acrylamide gels and blotted onto PVDF membrane (Immobilon-P). The protein blots were blocked with 5% nonfat milk in TBST. An appropriate amount of primary antibodies was added and incubated overnight at 4°C: Na$^+$/K$^+$-ATPase α1 polyclonal antibody (1:1000, ABL1141, Abbkine), rabbit anti-Flag-Tag antibody (1:1000, ab205606, Abcam). After washing, the membrane was incubated for another 1 h at room temperature with secondary antibodies: HRP-conjugated goat anti-rabbit IgG (H+L; 1:2000, AS014, ABclonal). The membrane was re-washed in TBST, developed with clarity western ECL substrate (Beyotime), and imaged on the Alliance Q9 Imager (Uvitec). Band intensities were determined using ImageJ software.

Western blot using animal tissues
We also performed a Western blot analysis according to the standard protocol described in our previous studies (Yu et al., 2019). Briefly,

proteins (40 μg/sample) were extracted from the brain of WT mice and PAC KO mice (RIPA, P0013B, Beyotime) and transferred onto PVDF membranes. The membranes were incubated at 4°C overnight with the customer-made primary rabbit PAC antibody (1:1000, ABclonal) or Beta Actin antibody (1:2000, 66009-1-Ig, Proteintech). Subsequently, the membranes were washed and incubated with the HRP-conjugated anti-rabbit IgG antibody (1:2000, A0216/A0208, Beyotime).

Anesthesia behavior
PAC KO mice and WT mice were weighed and labeled in groups. Chloral hydrate was intraperitoneally injected in two doses at 1.8 or 2.1 mmol/kg in two different batches of mice, respectively, because chloral hydrate has a narrow therapeutic dose range with the increased adverse effects with higher dosages (Pershad et al., 1999). The anesthesia behaviors were observed at room temperature of 18–20°C and relative humidity of 40−60%. After chloral hydrate injection, time recording was started with a stopwatch, and the induction time and duration time of anesthesia were observed and recorded. Induction time: the time between the injection of chloral hydrate and the appearance of loss of righting reflex in mice. Duration time: the time from the beginning of the righting reflex's loss to the righting reflex's recovery.

Electroencephalogram (EEG) recording
Mice were anesthetized (1% pentobarbital sodium, 4–5 mg/100 g body weight) and fixed on a brain stereotaxic apparatus. Then, we operated to remove the skin and soft tissues to expose the skull. One headmount was placed on the exposed skull and was glued with dental cement. During the headmount installing process, the dental adhesive was applied with a moistened fine brush so that the six-pin insertion hole on the headmount for connecting the preamplifier of the EEG acquisition system was kept clean and uncoated. The headmount was held tightly to the skull for several minutes until the dental cement dried by ultraviolet and the headmount had been firmly attached. The front edge of the headmount was placed at 3.2 mm in front of the fontanelle. The incision was washed with an antiseptic solution and sutured to prevent infection. The mouse was kept in a separate cage until the wound recovered. The EEG signals were recorded by the Pinnacle EEG Acquisition system and stored in a computer. The EEG data were exported in European data format (.EDF) by Pinnacle software and analyzed by MATLAB2018a.

Data analysis and statistics
TEVC and outside-out patch data were analyzed using pClampfit 10 (Molecular Devices) and Origin software 8.0. The conductances were calculated as macroscopic steady-state current divided by recording voltages. The conductance at 0 mV was estimated by the averaged conductance value measured at −20 and 20 mV. The Boltzmann function fitted the GV curves.

$$f(v) = \frac{G_{max}}{1 + e^{(V_{mid} - V)/V_c}} + C. \tag{1}$$

The conductance at different voltages and pH values were normalized to the maximal conductance values at pH 4.6 obtained by fitting the
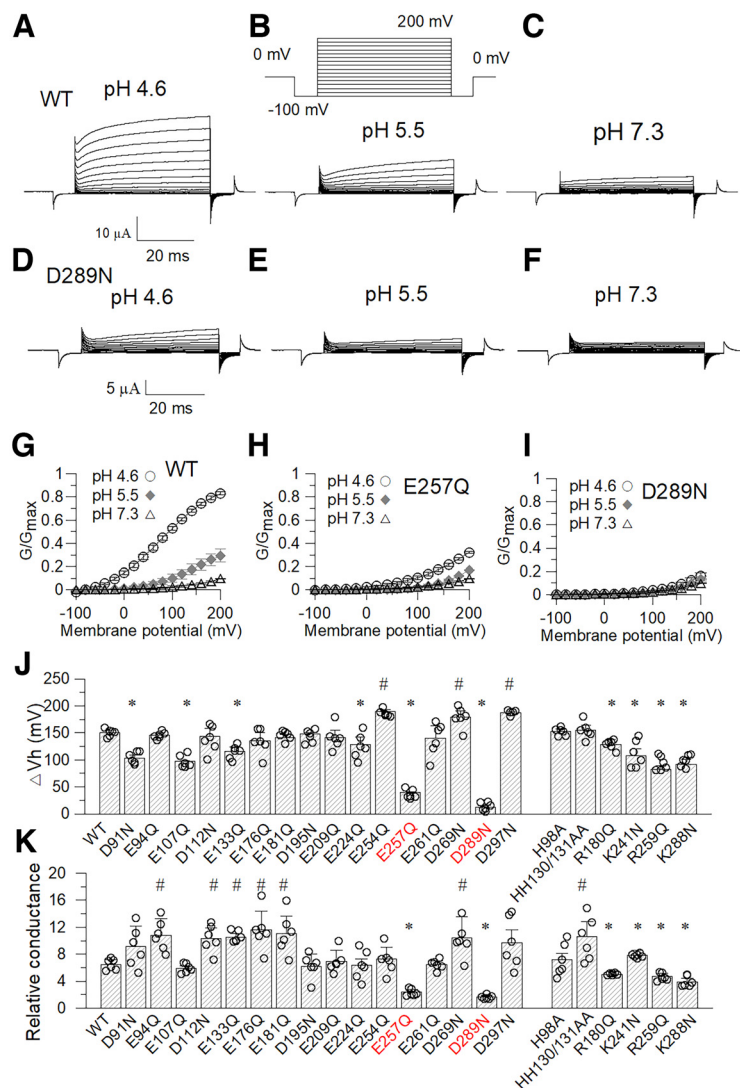

Figure 3. E257Q and D289N mutants abolished pH-dependent currents of the hPAC channel. *A–C,* The typical whole-cell current traces of the hPAC channel (WT) were recorded in the TEVC configuration. The cells were bathed with solutions at indicated pH values. *D–F,* The typical whole-cell current traces of the D289N mutant in bath solutions at displayed pH values. *G–I,* The plotted G-V curves of the hPAC WT channel, E257Q, and D289N mutants. *J,* The ΔV$_h$ values of the WT hPAC channel and mutants as listed. ΔV$_h$ was calculated as the V$_h$ values obtained at pH 5.5 minus the V$_h$ values of the same construct at pH 4.6. Data are expressed as mean ± SEM, $n \geqq 6$. *K,* Relative conductance values of the WT hPAC channel and its mutants at 200-mV depolarization. Data are expressed as mean ± SEM, $n \geqq 6$. The V$_h$ and relative conductance values of mutants are statistically lower than those of the WT hPAC channel labeled by *. The V$_h$ and relative conductance values of the mutants are statistically higher than the value of the WT channel labeled by #. The pH dependence of the WT hPAC channel and some mutants at 200-mV depolarization are shown in Extended Data Figure 3-1.

GV curves with the Boltzmann function for each patch. The maximal conductance was defined as the theoretical steady conductance obtained from the GV curves fitted by the Boltzmann function. For any single mutation, if the maximal conductance at pH 4.6 is equal to or ≥90% of the maximal conductance at pH 4.6 of the WT channel, the GVs were normalized to the maximal conductance of the mutant. Otherwise, the GVs were normalized to the average maximal conductance of the WT hPAC channel. For any double or triple mutations with A81C as background, if the maximal conductance at pH 4.6 is equal to or ≥90% of the maximal conductance of the A81C mutant, the GVs were normalized to their own maximal conductance. Otherwise, the GVs were normalized to the maximal conductance of A81C. The voltage at half activation of the hPAC channel was defined as V$_h$. The voltage of half activation between pH 4.6 and 5.5 is expressed as ΔV$_h$. We define the relative conductance of any given mutation as the ratio between conductance measured at pH 4.6 and the conductance measured at pH 7.3. Data in all

Table 1. V_h, $\triangle V_h$, and pH_{50} of the hPAC Channel mutants

	Vh at pH 4.6	Vh at pH 5.5	$\triangle$Vh (mean $\pm$ SEM)	pH_{50} at 200 mV	Patch numbers
WT	80.1 $\pm$ 1.1	225.4 $\pm$ 6.4	148.5 $\pm$ 5	5.16 $\pm$ 0.003	6
D91N	99.7 $\pm$ 0.8	202.8 $\pm$ 4.7	103.1 $\pm$ 5.6	5.63 $\pm$ 0.191	6
E94Q	85.1 $\pm$ 4.4	231.2 $\pm$ 10.5	146.1 $\pm$ 3.7	5.40 $\pm$ 0.029	6
H98A	89.1 $\pm$ 1.8	241.3 $\pm$ 5.4	152.2 $\pm$ 4.6	5.21 $\pm$ 0.048	6
K106N	105.9 $\pm$ 8.7	249.4 $\pm$ 7.9	143.5 $\pm$ 8.3	5.19 $\pm$ 0.005	6
E107Q	101.7 $\pm$ 6.1	199.2 $\pm$ 4.6	97.5 $\pm$ 0.9	5.71 $\pm$ 0.075	6
E107A	98.1 $\pm$ 3.6	169.8 $\pm$ 10.6	71.7 $\pm$ 8.9	5.70 $\pm$ 0.068	6
E107C	106.7 $\pm$ 6.9	214.3 $\pm$ 7.4	107.6 $\pm$ 10.2	5.38 $\pm$ 0.047	6
E107R	92.9 $\pm$ 7.6	156.2 $\pm$ 13.0	64.4 $\pm$ 8	6.02 $\pm$ 0.045	6
V108A	100.4 $\pm$ 9.7	208.8 $\pm$ 11.2	108.4 $\pm$ 10.1	5.23 $\pm$ 0.051	6
D109N	90.3 $\pm$ 4.7	250.3 $\pm$ 4.8	160.0 $\pm$ 5.9	5.19 $\pm$ 0.002	6
D112N	81.8 $\pm$ 7.8	225.0 $\pm$ 10.2	143.2 $\pm$ 14.8	5.43 $\pm$ 0.113	6
H130/131A	84.5 $\pm$ 6.2	239.2 $\pm$ 7.0	154.7 $\pm$ 9.7	5.32 $\pm$ 0.046	6
E133Q	105.7 $\pm$ 3.8	221.9 $\pm$ 6.4	116.2 $\pm$ 7.5	5.39 $\pm$ 0.055	6
E176Q	76.1 $\pm$ 4.7	212.0 $\pm$ 8.3	135.9 $\pm$ 14.8	5.26 $\pm$ 0.025	6
R180Q	77.5 $\pm$ 4.5	206.5 $\pm$ 8.8	128.9 $\pm$ 9.2	5.17 $\pm$ 0.019	6
E181Q	89.0 $\pm$ 0.1	230.4 $\pm$ 5.4	141.4 $\pm$ 5.9	5.16 $\pm$ 0.016	6
D195N	75.8 $\pm$ 5.5	224.0 $\pm$ 7.3	148.2 $\pm$ 2.3	5.38 $\pm$ 0.038	6
E209Q	80.3 $\pm$ 11.6	221.8 $\pm$ 12.5	141.5 $\pm$ 13.7	5.18 $\pm$ 0.005	6
E224Q	110.7 $\pm$ 8.0	239.5 $\pm$ 9.6	128.8 $\pm$ 13.3	5.38 $\pm$ 0.038	6
E250Q	104.2 $\pm$ 9.1	268.8 $\pm$ 7.9	164.6 $\pm$ 15.8	5.18 $\pm$ 0.005	6
E254Q	86.0 $\pm$ 4.9	275.8 $\pm$ 6.6	189.8 $\pm$ 3.7	5.16 $\pm$ 0.007	6
K241N	87.5 $\pm$ 9.7	195.6 $\pm$ 14.3	107.6 $\pm$ 13.2	5.15 $\pm$ 0.007	6
E257Q	294.6 $\pm$ 5.4	334.8 $\pm$ 6.8	40.2 $\pm$ 1.2	/	6
E257A	277.6 $\pm$ 9.4	313.5 $\pm$ 7.9	35.9 $\pm$ 2.3	/	6
E257C	288.2 $\pm$ 11.8	308.3 $\pm$ 11.2	21.7 $\pm$ 2.4	/	6
E257D	275.3 $\pm$ 12.5	306.4 $\pm$ 14.5	31.4 $\pm$ 2.2	/	6
R259Q	123.4 $\pm$ 7.6	205.8 $\pm$ 7.2	82.4 $\pm$ 7.3	5.42 $\pm$ 0.019	6
E261Q	103.6 $\pm$ 10.9	244.1 $\pm$ 19.3	140.5 $\pm$ 21.9	5.34 $\pm$ 0.059	6
D269N	88.5 $\pm$ 2.4	267.5 $\pm$ 3.5	179.0 $\pm$ 12.2	5.27 $\pm$ 0.071	6
K288N	144.2 $\pm$ 11.7	251.2 $\pm$ 12.8	107.6 $\pm$ 13.2	5.64 $\pm$ 0.045	6
D289N	306.0 $\pm$ 14.7	317.6 $\pm$ 6.9	11.6 $\pm$ 3.9	/	6
D289K	262.1 $\pm$ 11.7	305.1 $\pm$ 9.3	43.1 $\pm$ 2.9	/	6
D289E	244.3 $\pm$ 13.2	282.8 $\pm$ 10.5	38.5 $\pm$ 3.1	/	6
D289A	274.6 $\pm$ 15.1	313.0 $\pm$ 10.7	39.4 $\pm$ 2.5	/	6
D297N	93.2 $\pm$ 3.6	280.2 $\pm$ 5.4	187.0 $\pm$ 2.2	5.32 $\pm$ 0.119	6
P290A	96.2 $\pm$ 11.8	215.7 $\pm$ 16.5	119.7 $\pm$ 15.2	5.24 $\pm$ 0.023	6
Uninjected oocytes	293.3 $\pm$ 18.9	346.7 $\pm$ 22.5	53.4 $\pm$ 3.2	/	6

figures are shown as mean $\pm$ SEM. We used One-way ANOVA to do the statistical analysis among different constructs. Comparisons between the two groups of mice were made by t test; $p < 0.05$ was statistically significant.

The pH versus conductance curves were fitted by dose–response function as follows:

$$y = A1 + \frac{A1 - A2}{1 + 10^{(pH50 - x)p}}. \tag{2}$$

A1 is the normalized conductance at pH 7.3, A2 is the normalized conductance at pH 4.6. PH_{50} was defined as the pH value that reached the 50% of the conductance at pH 4.6.

We used MATLAB software to analyze the EEG signals. The EEG traces bandpass filter was set from 0.3 to 35 Hz. The components ratio of δ (0.4–4 Hz), θ (4–8 Hz), α (8–14 Hz), and β (14–30 Hz) were calculated. The unpaired t test was used to compare the ratios of different components in WT mice with the PAC channel KO mice. The $p < 0.05$ was considered statistically significant. Then heat maps were calculated using band power while a spectrum map was generated using the autocorrelation function. The data were shown as mean $\pm$ SEM.

Results

To dissect the pH-dependent activation mechanism of the hPAC channel, we first cloned and expressed the hPAC channel in *Xenopus* oocytes. Then, the currents were recorded by outside-out patches. The extracellular acidification and voltage-dependent macroscopic currents of the hPAC channel were observed (Fig. 1A–C). In contrast, only a slight pH-dependent current increase was observed in uninjected oocytes, probably from endogenous CLC-7 channels (Fig. 1D–F; Diewald et al., 2002). Then the GV curves were plotted and fitted with the Boltzmann function, which showed the enhanced conductance of the hPAC channel response to extracellular acidification and depolarization (Fig. 1G). The normalized conductance could be enhanced from 0% to 75% on 200-mV depolarization. Meanwhile, the voltage of half activation (V_h) of the hPAC channel decreases with the increase of extracellular proton concentrations (Fig. 1H). The V_h decreased by almost 300 mV when the extracellular pH value decreased from 7.3 to 4.6. To observe the hPAC channel currents more efficiently, we also used the TEVC recording method to record the hPAC channel currents in the oocytes. Huge currents (30–40 µA) were observed in the hPAC cRNA injected *Xenopus* oocytes, while only tiny currents (3–4 µA) were observed in uninjected oocytes (Fig. 1I,J). The plotted GVs show a big difference between the normalized conductance of the hPAC channel and the endogenous channels (Fig. 1K). These data indicate that the hPAC channel current can be observed in *Xenopus* oocytes without significant disturbance from endogenous currents. Thus, the *Xenopus* oocytes system can be used to examine the mechanism of the pH dependence of the hPAC channel.

Table 2. Relative conductance values of the hPAC channel mutants

	Relative conductance values (mean ± SEM)	Patch numbers		Relative conductance values (mean ± SEM)	Patch numbers
WT	6.5 ± 0.7	6	E257Q	2.3 ± 0.4	6
D91N	9.1 ± 3.0	6	E257A	1.8 ± 0.1	6
E94Q	10.8 ± 2.5	6	E257C	1.9 ± 0.1	6
H98A	7.2 ± 0.9	6	E257D	1.7 ± 0.2	6
K106N	6.5 ± 0.9	6	R259Q	4.7 ± 0.4	6
E107Q	5.9 ± 0.3	6	E261Q	6.5 ± 0.6	6
V108A	5.1 ± 1.0	6	D269N	10.4 ± 3.1	6
E107A	5.3 ± 0.4	6	K288N	3.9 ± 0.6	6
E107C	3.8 ± 0.3	6	D289N	1.6 ± 0.3	6
E107R	8.3 ± 1.4	6	D289K	2.1 ± 0.2	6
D109N	4.5 ± 0.6	6	D289E	2.8 ± 0.2	6
D112N	10.3 ± 1.6	6	D289A	1.9 ± 0.1	6
H130/131A	10.6 ± 1.2	6	D297N	9.7 ± 1.9	6
E133Q	10.5 ± 0.5	6	P290A	5.2 ± 0.5	6
E176Q	11.6 ± 2.7	6	A81C	2.3 ± 0.1	6
R180Q	5.0 ± 0.4	6	A81C/E107Q	2.8 ± 0.3	6
E181Q	11.1 ± 2.6	6	A81C/E224Q	2.3 ± 0.1	6
D195N	6.2 ± 1.8	6	A81C/E257Q	2.0 ± 0.2	6
E209Q	6.9 ± 1.7	6	A81C/E261Q	1.3 ± 0.1	6
E224Q	6.4 ± 0.9	6	A81C/D289N	2.0 ± 0.1	6
K241N	7.8 ± 0.7	6	A81C/E107A	3.7 ± 0.2	6
E250Q	4.6 ± 0.7	6	E107A/D289N	3.5 ± 0.3	6
E254Q	4.6 ± 0.8	6	A81C/E107A/D289N	1.8 ± 0.1	6
V256A	6.3 ± 0.6	6	uninjected oocyte	1.6 ± 0.1	6

Since the sensitivity of the PAC channel toward extracellular acidification is conservative in all species, the proton-sensitive sites are supposed to be among the conserved negative charged residues or histidine residues located in the extracellular domain of the PAC channel (Fig. 2A,B). In addition, the positively charged residues located at the intersubunit interface were also considered as potential pH-sensitive sites. Thus, we neutralized all conserved extracellular negative charged residues and alkalized residues at the intersubunit interface of the hPAC channel and recorded whole-cell currents of the WT hPAC channel. These mutants in two-electrode voltage-clamp configuration in Xenopus oocytes bathed with extracellular solutions at different pH values (Fig. 3A–F). For example, the D289N mutant lost almost the whole acidification-dependent currents of the hPAC channel, whose currents show no significant difference from those recorded from uninjected currents (Fig. 3D–F). The GV plots of the WT hPAC channel and its mutants exhibited the E257Q, and D289N mutants lost the acidification-dependent conductance enhancement (Fig. 3G–I). Although many mutants show statistically different ΔVh alteration from the ΔVh of the wild-type hPAC channel, only the E257Q and D289N mutants almost lose acidification-dependent ΔVh alteration between pH 5.5 and pH 4.6 (Fig. 3J,K; Table 1). We also plotted the normalized conductance versus pH value and obtained the pH_{50} value of these mutants (Extended Data Fig. 3-1A–C). Again, E257Q and D289N show a trivial conductance increase at pH 4.6, so the pH_{50} cannot be obtained (Extended Data Fig. 3-1D,E; Table 1). Considering the V_h at pH 7.3 of the WT channel and mutants may not be accurately estimated, and the pH_{50} cannot be obtained from E257Q, and D289N mutants, the ratio of the hPAC channel at pH 4.6 to the conductance at pH 7.3 is defined as the relative conductance to evaluate the acidification-dependent conductance alteration. Compared with the WT channel and other mutants, the E257Q and D289N almost lose relative conductance alteration on extracellular pH value change from 7.3 to 4.6. (Fig. 3K; Table 2). Despite some other positively charged mutants exhibiting statistically different relative conductance

with the wild-type channel, they still show pH-dependent activation. These results suggest that E257 and D289 are potential proton-sensitive sites.

But other explanations of these effects, including the possibility that these mutants alter the regular expression of the channel on the cell membrane or the mutants allosterically alter the acid-sensing of the hPAC channel, need to be tested (Fig. 3J,K; Table 2). We first tried a western blot in Xenopus oocytes to test these explanations. Although our antibody recognizes the hPAC channel well in mice tissues, we detected multiple bands in both the hPAC channel RNA injected and empty Xenopus oocytes. Thus, we dropped this method and tried to test the expression of these mutants on the plasma membrane by taking advantage of the temperature-dependent activation of the hPAC channel. When the temperature of the perfusion solution was enhanced from room temperature to 40°C, the current generated from the WT hPAC channel was enhanced more than two folds at pH 5.5 (Fig. 4A). Similarly, the E257Q and D289N mutants also exhibited strong temperature-dependent currents enhancement, indicating functional expression of these mutants on the cell membrane (Fig. 4B). Still, the uninjected oocytes did not exhibit temperature-dependent currents enhancement (Fig. 4C). Subsequently, we generated constructs in which the hPAC channel, D289N and E257Q mutants were fused with an EGFP protein at the end of the C-terminus. Then the constructs were transfected into HEK293T cells to express the hPAC-EGFP fusion protein in the cells. Forty-eight hours after transfection, the cells were stained by wheat germ agglutinin (WGA). The staining results showed that the EGFP fused WT hPAC channel, E257Q, and D289N mutants were expressed on the membrane, indicated by the green fluorescence (GFP) colocalized with the red fluorescence of WGA (membrane marker labeled by Alexa Fluor 594, red; Extended Data Fig. 4-1). The membrane expression levels of E257Q and D289N mutants, indicated by the colocalization rate of the WT channel, did not show a statistical difference from the membrane expression level of the WT hPAC channel (Extended Data Fig. 4-1). To avoid the EGFP-tag altering the hPAC channel
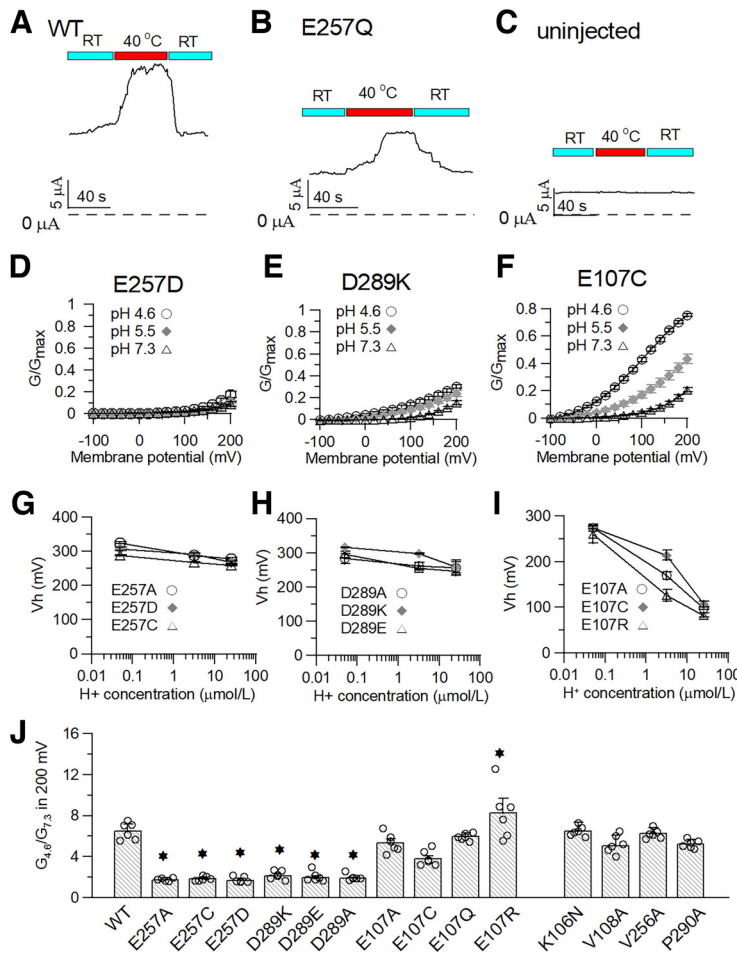
Figure 4. E257 and D289 mutants remove the pH sensitivity of the hPAC channel but maintain temperature-dependent activity. ***A–C***, Time courses of currents change of the WT, E257Q, and uninjected oocytes while the temperature of bath solution was enhanced from room temperature to 40℃. ***D–F***, Plotted GV curves of E257D, D289K, and E107C at different pH values, respectively. ***G, H***, The plotted V_h values of E257, D289, and E107 mutants at different pH, respectively. ***I***, The relative conductance values of E107, E257, and D289 mutants at 200 mV. ***J***, The relative conductance values of the mutants are statistically different from the WT channel are labeled by *. The membrane expression levels of the WT channel, E257Q, and D289N mutants were not substantially altered (Extended Data Fig. 4-1).

expression pattern, we generated a C-terminal Flag-tagged hPAC channel construct in pCDNA3.1 plasmids, which could be transfected into the HEK293T cells. Then the western blot was performed using the membrane proteins, which did not distinguish the cell plasma membrane from the internal membrane. The results showed that the E257Q and D289N mutants did not alter the expression level of the hPAC channel on the membrane (Fig. 5A,B). The same construct was also generated in the pGEMSH plasmid, and the synthesized RNAs were injected into the *Xenopus* oocytes. The western results showed that the E257Q and D289N also did not alter the expression level on the membrane in *Xenopus* oocytes (Fig. 5C,D). These results indicate that the E257Q and D289N mutants alter the acid sensitivity of the hPAC channel rather than influence the expression level of the hPAC channel mutants on the plasma membrane. Subsequently, we also mutated E257 and D289 to other amino acids to test whether the E257Q and D289N mutant allosterically altered the acidification-dependent activity of the hPAC channel. The sample GVs of the E257 mutants (E257D) and D289 mutants (D289K) did not show noticeable pH-dependent differences anymore, while the sample GV curves of the E107 mutants (E107C) still exhibited extracellular acidification-dependent

conductance enhancements (Fig. 4D,F). The acid-dependent V_h alteration values of E107 mutants are much larger than E257 and D289 (Fig. 4G–I; Table 1). Similarly, the relative conductance of E107 mutants in responses to extracellular acidification is much higher than the relative conductance of E257 and D289 mutants (Fig. 4J). Furthermore, we tested whether the E257 and D289 adjacent residue mutants also lose the acidification-dependent activation. The results showed the E257 and D289 adjacent residue mutants maintained the acidification-dependent relative conductance alteration (Fig. 4J), indicating these mutants do not allosterically affect the acidification-dependent channel activity. These results suggest the E257 and D289 residues are potential proton-sensitive sites of the hPAC channel.

To further test whether the E257 and D289 independently interact with proton or cooperate as an acid sensor, we first compared the subunit interface's local three-dimensional (3D) structure at pH 8 with the local 3D conformation at pH 4 based on a Cryo-EM study. The distance between D289 and E257 decreases from 8 Å to 3.6 Å when the extracellular pH value drops from 8 to 4 (Fig. 5E). This distance alteration implicates the cooperation of D289 and E257 for interaction with a proton. Then, we generated D289C/E257C double mutant and measured the current level at extracellular pH 7.3 and pH 4.6. The data showed that this double mutation produced a robust current at pH 7.3 on depolarization (Fig. 5F), while the single mutants E257C and D289C did not demonstrate a significant current on 200-mV depolarization even at pH 4.6 (Fig. 5G,H). However, the robust current in E257C/D289C double mutant could be abolished by the extracellular application of 50 mM DTT (Fig. 5I). In contrast, the double mutant H98C/E107C still show acidification-dependent activation (Fig. 5J). Furthermore, when the single mutant E257D or D289E removed the acidification-dependent activation, the acidification-dependent current could be observed in the double mutant E257D/D289E on depolarization (Fig. 5K). These data indicate that the E257 and D289 cooperatively interact with the proton to stabilize the PAC channel in an open conformation.

To test whether the A81C mutant of the hPAC channel, which exhibited robust currents at pH 7.3 while the gating still showed pH dependency (Fig. 6A–C; Ullrich et al., 2019), still use the same pH-sensitive site as the WT hPAC channel. Then we observed the current dependence on extracellular acidification of the A81C/E257Q and A81C/D289N. We found that on the background of A81C, the double mutant A81C/E257Q and A81C/D289N exhibited acidification-dependent activation (Fig. 6D,E). This result suggests that the E257 and D289 no longer play a role in pH sensitivity of the A81C mutant, because the pH-sensitive site and gating mechanism probably has been altered in this mutant. Thus, we tested whether other negative charged residues located at the hotspot of the subunit interface, predicted by previous CryoEM-structure, could alter the pH sensitivity of
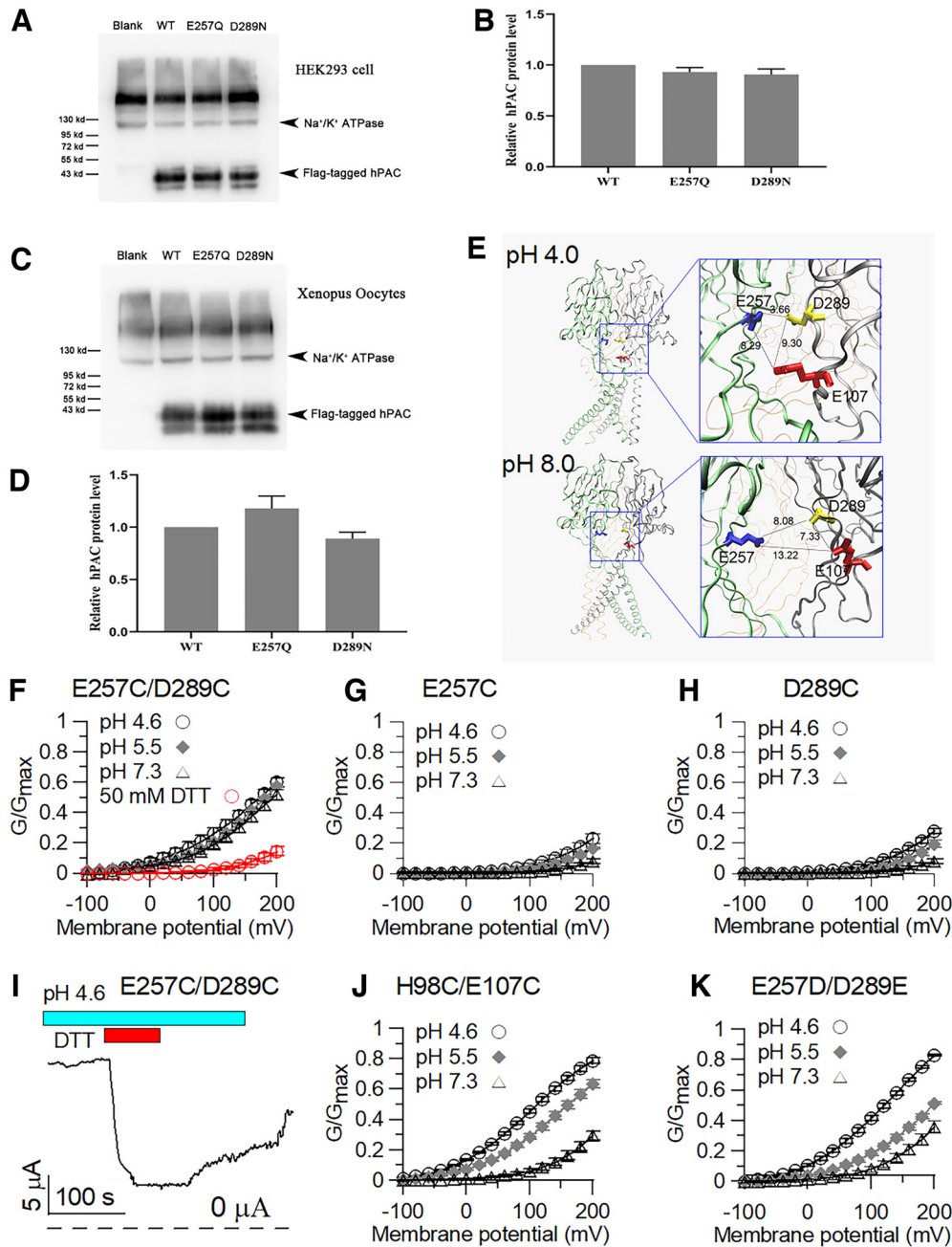
Figure 5. The disulfide bond formed between E257C and D289C stabilizes the opening conformation of the hPAC channel protein without proton binding. *A*, The conformation model of the hPAC channel based on the cryo-EM structure at pH 4 (left top) and pH 8 (left bottom) were shown, respectively. The enlarged local conformation of E257 (blue) on one subunit (green), D289 (yellow), and E107 (red) on its adjacent subunit (silver) were shown. The spatial distances among them were measured at pH 4 (right-top) and 8 (right-bottom). *B*, *C*, The Western blot results of the hPAC channel and its mutants using the plasma membrane protein in transfected HEK293T cells. *D*, *E*, The expression level of the hPAC channel and its mutants in the plasma membrane of *Xenopus* oocytes. *F*, The plotted GV curves of the double mutant E257C/D289C bathed in solutions at different pH and in solution at pH 4.6 applied with 50 mM DTT (red). *G*, *H*, The plotted GV curves of the single mutants E257C and D289C at different pH values. *I*, Time course of currents decline of E257C/D289C double mutant in solution at pH 4.6 response to 50 mM DTT application. *J*, *K*, The plotted GV curves of the double mutants H98C/E107C and E257D/D289E in bath solutions at indicated pH values.

the A81C mutant. Among them, we found that the double mutant A81C/E261Q lost the acidification-activated currents while the A81C/E224Q maintained normal acidification-dependent activation (Fig. 6F–I; Extended Data Fig. 3-1F). As a result, the V_h change and relative conductance of the A81C/E261Q mutant exhibit minimal pH dependence (Fig. 6J,K). These results indicate that the A81C mutant and the WT hPAC channel use different pH-sensitive sites to activate the hPAC channel.

Since we are interested in the role of the hPAC channel in anesthesia and hypnosis, we tested several general anesthetic effects

on the activation of the hPAC channel. Among them, we found that chloral hydrate activated the hPAC channel in a dose-dependent manner when applied in a pH 5.5 bath solution. Upon depolarization to 200 mV, the total current could be enhanced more than two folds when 50 mM chloral hydrate is extracellularly applied while 100 mM chloral hydrate did not induce endogenous current change on the osmolarity change from 307 to 377 Osm (Fig. 7A–E). The half effective dose concentration (EC_{50}) was around 22 mM based on the Hill equation fit of the activation data (Fig. 7F). The chloral hydrate's activation effect (fitted EC_{50})
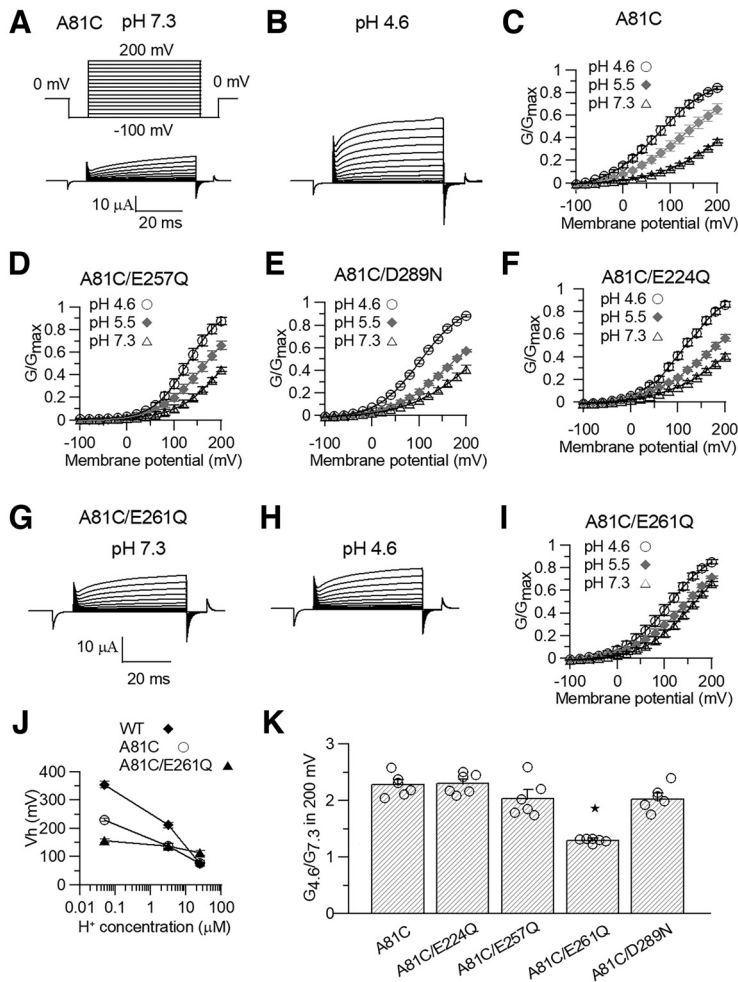
Figure 6. In the background of the A81C mutant, the E261Q removes the pH-dependent activity rather than E257Q and D289N mutants. ***A***, ***B***, TEVC recorded the sample current traces of A81C mutant in a solution at indicated pH values. ***C–F***, The plotted GV curves of the mutants A81C, A81C/E257Q, A81C/D289N, and A81C/E261Q. ***G***, ***H***, TEVC recorded the typical current traces of the A81C/E261Q mutant in the solution at indicated pH values. ***I***, The plotted GV curves of the mutants A81C/E224Q. ***J***, The plotted V_h values of the WT hPAC, A81C, and A81C/E261Q mutants at different pH. ***K***, The ΔV_h of the indicated mutants from pH 7.3 to pH 4.6. The relative conductance values of mutants A81C, A81C/E224Q, A81C/E257Q, A81C/E261Q, and A81C/D289N at 200 mV. The relative conductance of mutants was compared with the conductance of wild-type channels by t test; *$p < 0.05$.

exhibited weak voltage dependence (Fig. 7*G*). The activation time course showed relatively fast activation effects, probably depending on the perfusion speed and bath solution exchanging time (Fig. 7*H*). Interestingly, both the E257C/D289C double mutation and A81C mutation abolished the chloral hydrate activation effect of the hPAC channel, while the double-cycle E257D/D289E mutation maintained the activation effect of the chloral hydrate (Fig. 7*H–K*). The EC_{50} value of chloral hydrate in the E257D/D289E mutant is close to the value in the WT hPAC channel (Fig. 7*L*). These results indicate the activation effect of chloral hydrate probably relies on the integrity of the pH-sensitive site of the hPAC channel. Thus, we tested the activation effect of chloral hydrate in extracellular solutions at pH 7.3 and 4.6. Chloral hydrate did not demonstrate the activation effect on the hPAC channel at pH 7.3 (Fig. 8*A*), while the activation effect of chloral hydrate was also attenuated at extracellular pH 4.6 but with a lower EC_{50} ($EC_{50} = 1.4 \pm 0.3$ mM, Fig. 8*B,C*). The activation effects of the chloral hydrate were also weakly voltage-dependent in pH 4.6 (Fig. 8*D*). These data suggest that the activation effect of chloral hydrate is most potent in slightly acidic conditions.

To further certify the physiological consequence of the PAC channel activation by chloral hydrate in anesthesia and hypnosis, we generated PAC channel knock-out mice using the CRISPR/Cas9 strategy (Fig. 9*A*). The genotype was confirmed by PCR and Western Blotting (Fig. 9*B,C*). Then we compared the hypnotic effect of the PAC knock-out mice with the wild-type littermates. The results showed the hypnotic effect of chloral hydrate in the KO mice was significantly less potent than in the WT mice. Upon intraperitoneal injection of either (1.8 mm/kg) or (2.1 mm/kg) chloral hydrate, the KO mice exhibited a longer induction time for loss of righting reflex (LORR) than WT mice (Fig. 9*D*). Also, the LORR duration time of the KO mice was significantly shorter than the WT mice (Fig. 9*E*). The anesthesia state alteration was further confirmed by electroencephalogram recording (EEG), which showed the more bursting discharges during the induction time and anesthesia state in the KO mice (Fig. 9*F,G*). The energy analysis of the EEG also indicated a lower power intensity in low-frequency oscillations in the KO mice anesthetized by chloral hydrate (Fig. 9*H*, KO mice in red vs WT mice in blue). The statistical analysis of EEG showed the lower power of δ waves and higher intensity of α waves in KO mice than waves in WT mice (Fig. 9*I*). These data indicate the PAC channel is probably a target of chloral hydrate.

Discussion

This study identified a proton-sensitive site of the hPAC channel, composed of E257 and D289 residues. The first evidence is that the E257 and D289 mutants exhibit similar effects on removing the acidification-dependent currents as the D289N and E257Q mutations did. In contrast, H98 and E107 mutants do not display the disruption of the acidification-dependent current of the hPAC channel. These results are not consistent with the idea that the H98 and E107 of the hPAC channel coordinately form one proton binding site. The 3D structure determined by cryo-EM indicated that the E257 residue in one subunit is spatially close to the D289 residue in the adjacent subunit. It raises the possibility that these two residues coordinately form one proton-sensitive site (Fig. 5). If so, we expect that the double mutant E257C/D289C allows the E257C and D289C in adjacent subunits to form a disulfide bond to exhibit a similar activating effect on the hPAC channel as the proton binding does. Indeed, the double mutant demonstrates an effect for disrupting the acidification-dependent current but remains channel activity at pH 7.3 on depolarization. Furthermore, the mutant cycle analysis shows exchanging negatively charged residue E257 and D289 maintains the pH sensitivity of the hPAC channel when single mutants E257D and D289E remove the pH sensitivity of the hPAC channel. These data further support the E257 and D289 cooperatively forming a proton-sensitive site. However, on the background of the A81C mutant, which shows basal level currents at pH 7.3, the double mutants A81C/D289N and A81C/E257Q no longer disrupt the acid-dependent currents.
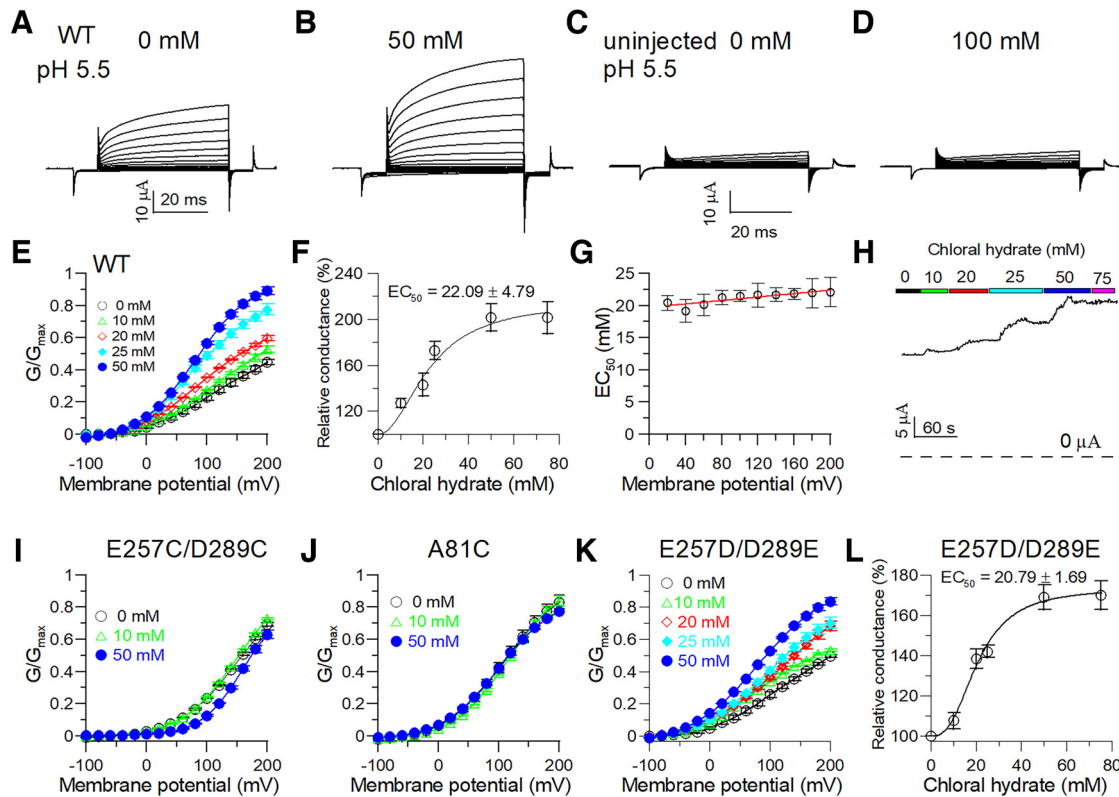
Figure 7. Chloral hydrate activates the hPAC channel by stabilizing the pH-dependent activation conformation. ***A, B***, The sample current traces of the WT hPAC in the perfusion solution at pH 5.5 were perfused with 0 (***A***) or 50 (***B***) mM chloral hydrate as indicated. ***C, D***, The sample traces of the uninjected oocytes with 0 (***C***) or 100 (***D***) mM chloral hydrate. ***E***, The plotted GV curves of the hPAC channel at different concentrations of chloral hydrate. The conductance values are normalized to maximal conductance (G_{max}) at 200 mV with 50 mM chloral hydrate application. ***F***, The Hill equation fit of the activation of chloral hydrate in 200 mV ($EC_{50} = 22.09 \pm 4.79$ mM, coefficient factor = 1.9 ± 0.9). ***G***, EC_{50} values show weak voltage dependence from 20- to 200-mV depolarization. ***H***, The activation time course of the hPAC channel response to different concentrations of chloral hydrate at pH 5.5. ***I–K***, The plotted GV curves of E257C/D289C, A81C, and E257D/D289E mutants in solution with different concentrations of chloral hydrate. ***L***, The Hill equation fit of the activation effect of chloral hydrate on E257D/D289E mutants at 200 mV ($EC_{50} = 20.79 \pm 1.69$ mM, coefficient factor = 2.78 ± 0.68).

But the E261Q disrupts the acid-dependent current of the A81C mutant. These data probably demonstrated the backbone mutant could alter the pH-sensitive site. The E261 residue is also located in the hotspot of the pH-sensitive site predicted by the Cryo-EM structure (Deng et al., 2021). Thus, in our conclusion, in the wild-type hPAC channel, the E257 and D289 residues form a pH-sensitive site. But on the background of A81C, the E261Q mutant disrupts the pH dependent gating probably because of a local structure alteration. Interestingly, among the PAC channels in different species, the human, mole-rat, chicken, and zebrafish PAC channels do not show significant current at pH 7.4, but the green anole PAC channel exhibits robust currents at pH 7.4. Our results implies that the green anole PAC channel may use different pH-sensitive sites from PAC channels in other species.

However, another two studies are published during the preparation of this manuscript. One study claims that neutralizing a series of residues, including
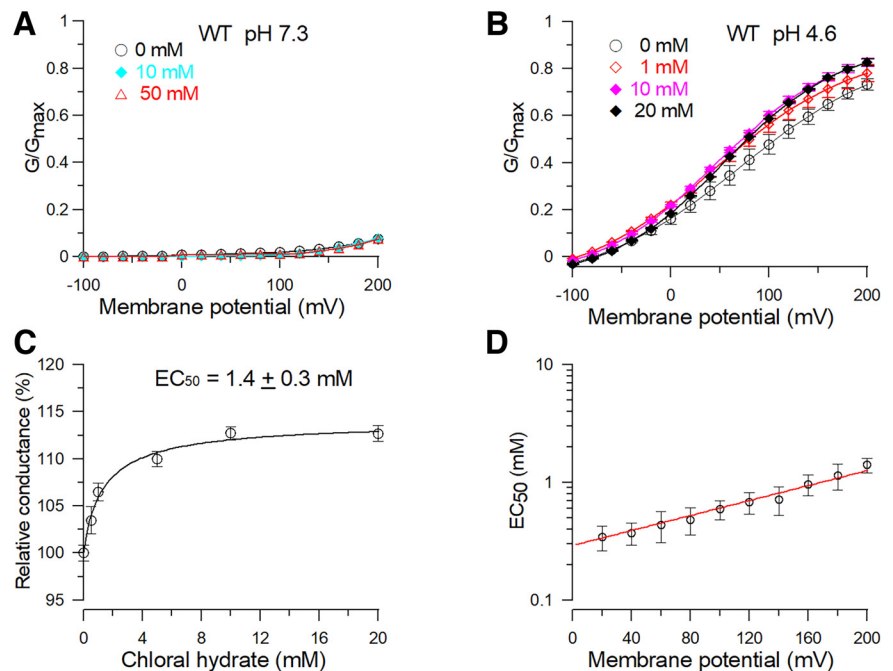

Figure 8. The activation effect of chloral hydrate on the hPAC channel at pH 4.6 and 7.3. ***A***, The plotted GV curves of the hPAC channel at pH 4.6 with different concentrations of chloral hydrate. The conductance values are normalized to maximal conductance (G_{max}) at 200 mV with 20 mM chloral hydrate. ***B***, The Hill equation fit of the activation of chloral hydrate at 200 mV ($EC_{50} = 1.4 \pm 0.3$ mM, coefficient factor = 0.9 ± 0.2). ***C***, EC_{50} values show weak voltage dependence from 20- to 200-mV depolarization. ***D***, The plotted GV curves of the hPAC channel at different concentrations of chloral hydrate at pH 7.3.
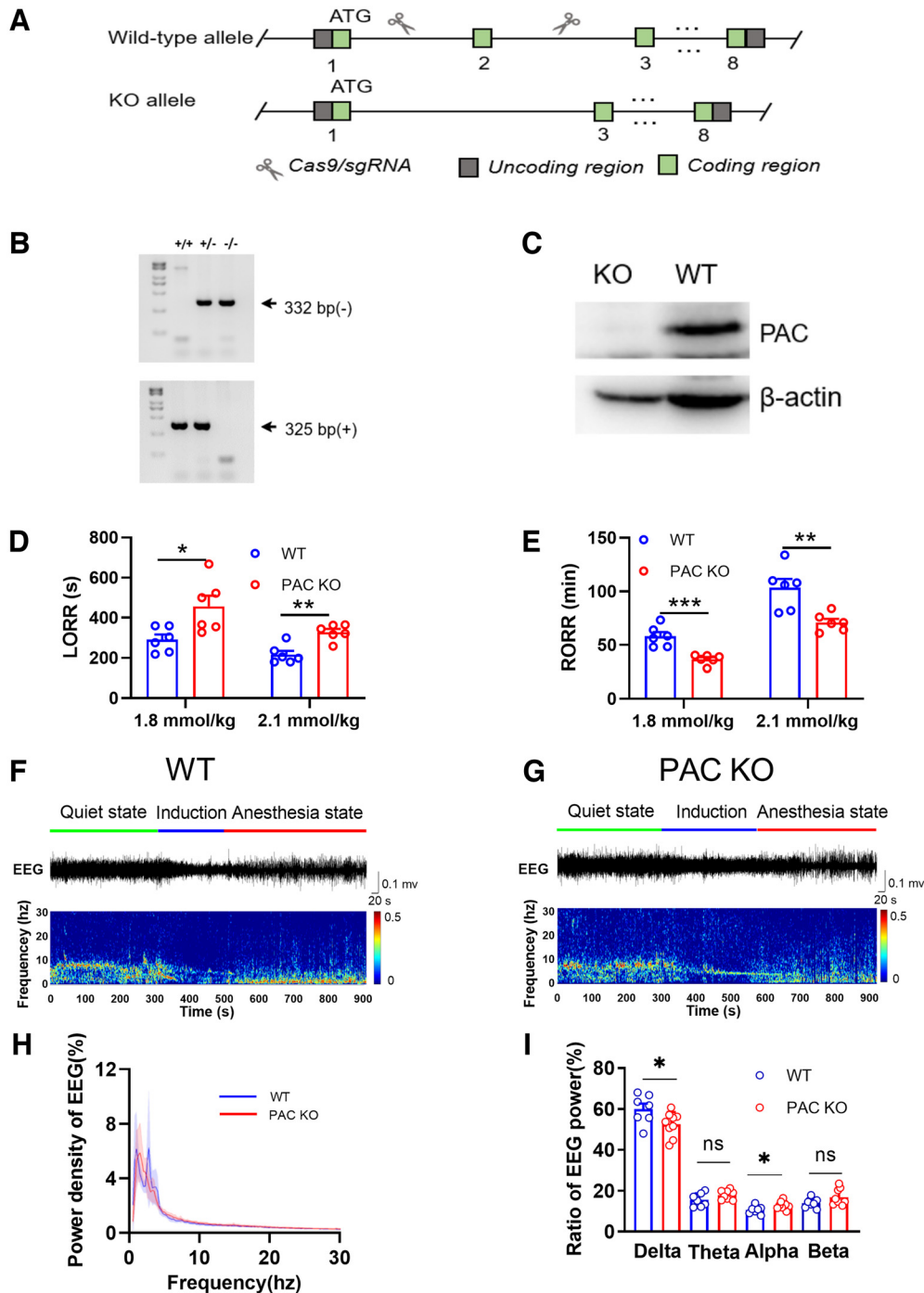
Figure 9. The PAC channel KO mice are resistant to chloral hydrate anesthesia. ***A***, The schematic diagram of the PAC channel knock-out strategy. Exon2 of the TMEM206 gene is targeted as the knock-out region. The exon2 region contains a 97-bp coding sequence. The deletion of the region results in disruption of the PAC transcript. ***B***, Genotyping of mice by PCR method. The wild-type (+/+), heterozygous (+/−), and homozygous knock-out genotype (−/−) were identified by PCR amplification using mouse tail genomic DNA as a template. ***C***, Representative western blot analysis of PAC protein expression in the brain tissues extracted from wild-type mice and PAC (−/−) mice. ***D***, PAC KO mice exhibit longer induction time ($p < 0.05$, WT induction time: 291.17 ± 19.94 s; PAC KO induction time: 476.5 ± 55.73 s) under intraperitoneal injection of 1.8 mmol/kg body weight chloral hydrate and longer induction time than WT mice with an intraperitoneal injection of 2.1 mmol/kg body weight chloral hydrate ($p < 0.01$, WT induction time: 216.33 ± 13.69 s; PAC KO induction time: 300.5 ± 22.84 s). ***E***, The PAC KO mice show shorter duration time than WT mice (1.8 mmol/kg: $p < 0.001$, WT duration time: 58.04 ± 3.13 min; PAC KO duration time: 36.68 ± 1.46 min; 2.1 mmol/kg: $p < 0.01$, WT duration time: 103.33 ± 6.76 min; PAC KO duration time: 71 ± 2.68 min). ***F***, ***G***, Typical traces and heat maps of electroencephalogram (EEG) recording of WT mice (***F***) and PAC KO mice (***G***) cover the whole anesthesia process induced by chloral hydrate at 1.8 mmol/kg. ***H***, Power spectrums in two groups of mice under 1.8 mmol/kg chloral hydrate anesthesia. ***I***, The ratios of categorized waves in the EEG between WT and PAC KO mice.

H98A, E107Q, H131A, E224Q, D289N, and D297N, reduces the proton activation hPAC channel. H131, E224, D289, and D297 are implicated in proton sensing in the PAC channel based on the coefficient factor of the Hill equation close to 4 (Cai et al., 2021). But we would like to argue that some mutations that the authors claimed to reduce proton-activated current are not valid, such as H98, E107, H131, E224, and D297. In addition, the authors missed the E257Q, which dramatically reduces the

acidification-activated currents. A possible reason for these mistakes is that the authors' protocol only reached 80 mV depolarization, at which some mutant channels have not begun to activate even in pH 4.6 solution because of the rightward shift in the voltage dependency. For example, the V_h values of E224Q (110 ± 8 mV; Table 1) and E107Q (101 ± 6 mV; Table 1) are much higher than the value of the WT hPAC channel (80 ± 1 mV). Since the channel activity is both pH and voltage-dependent, the Hill coefficient cannot predict the numbers of protons bound to the hPAC channel. Another study also used cryo-EM to dissect the proton sensor. It indicated two pairings of proton-mediated carboxyl-carboxylate interactions occur between residues on adjacent subunits (E249 to E107 and E257 to D289), and the third (E250 to D297) is between residues of the same subunit (C. Wang et al., 2022). The electrophysiology data in this study demonstrated the normalized current levels of these mutants at other pH values to the current levels at pH 4.5 and showed that the E257 and D289 mutants exhibit minimal currents but the neutralized mutants maintained pH-dependent currents. However, in our data, the mutants lose pH-dependent current but are still functional because the temperature-dependent macroscopic currents were not influenced. These data indicate the pH and temperature independently control the gating of the hPAC channel. Furthermore, the protocol of this study also only depolarized to 60 mV, at which some mutants do not demonstrate proton-activated currents. The Boltzmann equation is a suitable function for describing the conductance alteration on pH and voltage change of the hPAC channel, by which the pH dependence could be reflected as V_h values change as it has been used to describe other voltage and pH-sensitive channels, such as Slo3 (Tang et al., 2010; G.M. Wang et al., 2020). In our study, the depolarization reached 200 mV, at which the relative conductance of the PAC channel between pH 4.6 and pH 7.3 was calculated. In addition, the V_h alteration between pH 5.5/pH 7.3 and pH 4.6 was also used to evaluate pH dependence alteration. Thus, we believe our results are sound. However, all our biophysical data were obtained from *Xenopus* oocytes, maintained at 16°C, a condition that facilitates the protein folding and membrane trafficking of the hPAC channel. Thus, it may not represent the hPAC expression pattern in mammalian cells because the hPAC channel also functions in the endosome (Osei-Owusu et al., 2021).

Interestingly, the chloral hydrate can dose-dependently activate the hPAC channel in a pH-dependent way. Either disrupting the pH-sensitive site (E257Q or D289N) or shifting the pH-sensitive site (A81C) cancels the activation effect of chloral hydrate, whereas the mutant (E257D/D289E) that possesses the function of the pH-sensitive site maintains the activation effect of chloral hydrate on the hPAC channel. Thus, we propose that the chloral hydrate activates the hPAC channel by stabilizing the open channel conformation created by a proton binding with the hPAC channel. The attenuated activation effect of chloral hydrate in the condition of pH 4.6 suggests a high concentration of protons could replace the role of chloral hydrate, which implicates the chloral hydrate interacts with and activates the hPAC channel in the absence of proton binding. Thus, the dynamic activation process by chloral hydrate needs the initial activation of the hPAC channel by proton binding, following a chloral hydrate binding and stabilizing the open conformation of the channel even when the proton dissociates with the channel. But how the chloral hydrate interacts with the hPAC channel to stabilize the open conformation remains further explored.

The pH-dependent activation of the hPAC channel by chloral hydrate may have physiological consequences because chloral hydrate is acidic (pH 3.5–5.5) when dissolved in normal saline. When used as an anesthetic, it also significantly decreased the arterial pH value (300 mg/kg, −1.69, 400 mg/kg, −2.31 in rats; Field et al., 1993). If we consider the PAC channel as the drug target of chloral hydrate, the chloral hydrate concentration must reach the concentration that can significantly activate the PAC channel when used as an anesthetic. The clinically used chloral hydrate dose could be 20 mg −100 mg/kg up to 1 g/dose for infants and 2 g/dose for older children (Davis, 2020). Based on a measured 1.4 μM plasma concentration of chloral hydrate in male adults who orally took one-dose 1500 mg chloral hydrate (Merdink et al., 2008), the clinically used chloral hydrate plasma concentration (20–100 mg/kg, hypothesizing average adult body weight is 75 kg) is 14–70 μM. Another study gave a much lower plasma concentration of 0.4 μM (65 ng/ml) when the 50 mg/kg chloral hydrate was orally taken (Humbert et al., 1994). In these conditions, the chloral hydrate concentration is far from activating the PAC channel. However, in experimental animals (mice), the chloral hydrate was used in higher concentrations. The measured chloral hydrate blood concentration is 2 mM in mice with an intravenous 300 mg/kg injection (Abbas et al., 1996; Vitello et al., 2015). The concentration is much higher than the EC_{50} (1.4 mM; Fig. 6) of chloral hydrate activating the PAC channel at pH 4.6. Thus, in our study, intraperitoneally injected 1.8 mm/kg (300 mg/kg)–2.1 mm/kg (400 mg/kg) chloral hydrate in mice permits the accumulation of a higher blood chloral hydrate concentration with resultant activation of the PAC channel (considering the arterial pH value is close to 5). Consistent with this calculation, our data clearly show deletion of the PAC channel in mice significantly attenuated the hypnic effect of the chloral hydrate. Traditionally, the hypnic role of the chloral hydrate is attributed to its metabolite, trichloroethanol, to activate the GABAa receptor (Pistis et al., 1997). Therefore, our data identify the PAC channel as a new target for chloral hydrate playing its role.

In summary, our results support the idea that E257 and D289 residues cooperatively form a pH-sensitive site but argue against the view that H98 and E107 are involved in pH sensing in the hPAC channel. Our data also suggest that the chloral hydrate activates the hPAC channel by stabilizing an open conformation initiated by the proton-bound in the hPAC channel. Consequently, the chloral hydrate probably plays its hypnic role by activating the PAC channel. Thus, our results provide new insights into the mechanism of pH sensitivity of the hPAC channel and the chloral hydrate activation of the hPAC channel, which also contributes to future studies on the function of the PAC channel.

References

Abbas RR, Seckel CS, Kidney JK, Fisher JW (1996) Pharmacokinetic analysis of chloral hydrate and its metabolism in B6C3F1 mice. Drug Metab Dispos 24:1340–1346.

Cai R, Tang J, Chen XZ (2021) Ion permeation controlled by hydrophobic residues and proton binding in the proton-activated chloride channel. iScience 24:103395.

Davis PW (2020) Pfenninger and Fowler's procedures for primary care. San Diego: Elsevier, Inc.

Deng Z, Zhao Y, Feng J, Zhang J, Zhao H, Rau MJ, Fitzpatrick JAJ, Hu H, Yuan P (2021) Cryo-EM structure of a proton-activated chloride channel TMEM206. Sci Adv 7:eabe5983.

Diewald L, Rupp J, Dreger M, Hucho F, Gillen C, Nawrath H (2002) Activation by acidic pH of CLC-7 expressed in oocytes from *Xenopus laevis*. Biochem Biophys Res Commun 291:421–424.

Field KJ, White WJ, Lang CM (1993) Anaesthetic effects of chloral hydrate, pentobarbitone and urethane in adult male rats. Lab Anim 27:258–269.

Humbert L, Jacquemont MC, Leroy E, Leclerc F, Houdret N, Lhermitte M (1994) Determination of chloral hydrate and its metabolites (trichloroethanol and trichloracetic acid) in human plasma and urine using electron capture gas chromatography. Biomed Chromatogr 8:273–277.

Kittl M, Helm K, Beyreis M, Mayr C, Gaisberger M, Winklmayr M, Ritter M, Jakab M (2019) Acid- and volume-sensitive chloride currents in microglial cells. Int J Mol Sci 20:3475.

Lambert S, Oberwinkler J (2005) Characterization of a proton-activated, outwardly rectifying anion channel. J Physiol 567:191–213.

Merdink JL, Robison LM, Stevens DK, Hu M, Parker JC, Bull RJ (2008) Kinetics of chloral hydrate and its metabolites in male human volunteers. Toxicology 245:130–140.

Osei-Owusu J, Yang J, Leung KH, Ruan Z, Lü W, Krishnan Y, Qiu Z (2021) Proton-activated chloride channel PAC regulates endosomal acidification and transferrin receptor-mediated endocytosis. Cell Rep 34:108683.

Pershad J, Palmisano P, Nichols M (1999) Chloral hydrate: the good and the bad. Pediatr Emerg Care 15:432–435.

Pistis M, Belelli D, Peters JA, Lambert JJ (1997) The interaction of general anaesthetics with recombinant GABAA and glycine receptors expressed in *Xenopus laevis* oocytes: a comparative study. Br J Pharmacol 122:1707–1719.

Ruan Z, Osei-Owusu J, Du J, Qiu Z, Lü W (2020) Structures and pH-sensing mechanism of the proton-activated chloride channel. Nature 588:350–354.

Tang QY, Zhang Z, Xia XM, Lingle CJ (2010) Block of mouse Slo1 and Slo3 K+ channels by CTX, IbTX, TEA, 4-AP and quinidine. Channels (Austin) 4:22–41.

Tang QY, Zhang FF, Xu J, Wang R, Chen J, Logothetis DE, Zhang Z (2016) Epilepsy-related slack channel mutants lead to channel over-activity by two different mechanisms. Cell Rep 14:129–139.

Ullrich F, Blin S, Lazarow K, Daubitz T, von Kries JP, Jentsch TJ (2019) Identification of TMEM206 proteins as pore of PAORAC/ASOR acid-sensitive chloride channels. Elife 8:e49187.

Vitello DJ, Ripper RM, Fettiplace MR, Weinberg GL, Vitello JM (2015) Blood density is nearly equal to water density: a validation study of the gravimetric method of measuring intraoperative blood loss. J Vet Med 2015:152730.

Wang C, Polovitskaya MM, Delgado BD, Jentsch TJ, Long SB (2022) Gating choreography and mechanism of the human proton-activated chloride channel ASOR. Sci Adv 8:eabm3942.

Wang GM, Zhong ZG, Du XR, Zhang FF, Guo Q, Liu Y, Tang QY, Zhang Z (2020) Cloning and characterization of the rat Slo3 (KCa 5.1) channel: from biophysics to pharmacology. Br J Pharmacol 177:3552–3567.

Yang J, Chen J, Del Carmen Vitery M, Osei-Owusu J, Chu J, Yu H, Sun S, Qiu Z (2019) PAC, an evolutionarily conserved membrane protein, is a proton-activated chloride channel. Science 364:395–399.

Yu JT, Liu Y, Dong P, Cheng RE, Ke SX, Chen KQ, Wang JJ, Shen ZS, Tang QY, Zhang Z (2019) Up-regulation of antioxidative proteins TRX1, TXNL1 and TXNRD1 in the cortex of PTZ kindling seizure model mice. PLoS One 14:e0210670.

Zhang L, Liu SY, Yang X, Wang YQ, Cheng YX (2020) TMEM206 is a potential prognostic marker of hepatocellular carcinoma. Oncol Lett 20:174.

Zhao J, Zhu D, Zhang X, Zhang Y, Zhou J, Dong M (2019) TMEM206 promotes the malignancy of colorectal cancer cells by interacting with AKT and extracellular signal-regulated kinase signaling pathways. J Cell Physiol 234:10888–10898.